




Article

Momentum Transfer in Short-Channel Structures of Hexagonal Channel Cross-Section Shape: Experiments vs. CFD

Katarzyna Sindera ^{1,*} , Marzena Iwaniszyn ¹  and Przemysław J. Jodłowski ² 

¹ Institute of Chemical Engineering, Polish Academy of Sciences, 44-100 Gliwice, Poland; miwaniszyn@iich.gliwice.pl

² Faculty of Chemical Engineering and Technology, Cracow University of Technology, 31-155 Kraków, Poland; pjodlowski@pk.edu.pl

* Correspondence: katarzyna.sindera@iich.gliwice.pl; Tel.: +48-32-231-08-11

Abstract: Short-channel structures are promising catalyst carriers because it is easy to control the heat/mass transfer and fluid flow characteristics by changing their lengths. In this work, the flow resistance of hexagonal structures was investigated experimentally and numerically. The structure tested (6 mm long) was manufactured from AISI 316 steel using the selective laser melting technique. Due to some differences between theoretical approaches and practical results, two types of computational models were applied to analyze the pressure distribution in a short hexagonal duct. It was shown that although experimental results agree with some theoretical solutions, the channel wall thickness should not be omitted from the overall flow resistance. A comparison of short structures differing in channel length with widely used long monoliths was performed as well.

Keywords: short-channel structures; pressure drop; computational fluid dynamics



Citation: Sindera, K.; Iwaniszyn, M.; Jodłowski, P.J. Momentum Transfer in Short-Channel Structures of Hexagonal Channel Cross-Section Shape: Experiments vs. CFD. *Catalysts* **2021**, *11*, 1036. <https://doi.org/10.3390/catal11091036>

Academic Editor: Ruoyu Hong

Received: 12 July 2021

Accepted: 23 August 2021

Published: 27 August 2021

Publisher's Note: MDPI stays neutral with regard to jurisdictional claims in published maps and institutional affiliations.



Copyright: © 2021 by the authors. Licensee MDPI, Basel, Switzerland. This article is an open access article distributed under the terms and conditions of the Creative Commons Attribution (CC BY) license (<https://creativecommons.org/licenses/by/4.0/>).

1. Introduction

Nowadays, many harmful substances are still released into the atmosphere. Examples of such emissions are: methane, nitrogen oxides, sulfur oxides, volatile organic compounds and particulate matter (PM_{2.5} and PM₁₀). The effects of such emissions are significant both for the environment and for the organisms living in it. The IARC (International Agency for Research on Cancer) has classified air pollution in the first, most harmful group of carcinogenicity [1]. It has been estimated that around 3.22 million people died globally as a result of diseases caused by air pollution in 2010 alone [2].

Catalytic processes are able to effectively remove dangerous substances. Heterogeneous catalysts are of particular importance here [3]. Structured reactors are manufactured and used on a large scale in the treatment of emissions from gasoline and diesel engines to steam reforming of natural gas. However, in view of the growing needs and still-developing industry, there is an increasing necessity to search for new, more effective types of catalysts. Taking into account the annual global production of cars (50 million units) and the estimated increase in the number of used cars in the world (which will reach about 1.3 billion units in 2030 [4]), it seems particularly important to address this problem.

In the case of structured reactors, catalytic filling consists of the active phase and the support. The active phase is responsible for the course of the reaction. However, it often consists of expensive noble metals such as platinum, palladium or rhodium. For this reason, only a thin active phase layer is applied to the surface of the carrier. The geometry of the carrier is therefore particularly important. Effective catalyst support should provide intensive heat/mass transport and adequate availability of active centers for fluid molecules without generating high diffusional resistance. In order to deposit a significant amount of the active phase on the carrier surface, a large specific surface area S_v is desirable. High porosity ϵ of the support will lower the flow resistance, which leads to a reduction in pumping costs. Currently, the most commonly used industrial carriers

are monoliths and packed beds. Monoliths, used in exhaust gas treatment of vehicles, may provide an eligible porosity (about 0.83) and a large specific surface area (up to about $4000 \text{ m}^2 \cdot \text{m}^{-3}$) [5]. They ensure a very low flow resistance but they also have very poor transport properties. This is especially problematic for fast catalytic reactions, where the diffusion resistances limit the overall process rate. Packed beds can be used in the form of granules, spheres, rings, etc. A grain size of 2–10 mm is most commonly used. Packed beds allow the achievement of much more favorable values of transport coefficients than monoliths, but they also cause a significantly larger flow resistance, resulting from their low porosity.

Both of these types of carriers have many drawbacks that may be overcome by using new ones. The research described in this paper focuses on a new type of catalytic carriers called short-channel structures, which was proposed by Kołodziej et al. [6,7]. The idea of the support is based on the theory of developing laminar flow [8]. When the gas enters the long monolithic channels, the flow quickly develops within a very short distance from the channel's inlet. Therefore, the fully developed laminar flow exists over most of the channel's length, resulting in a weak heat/mass transfer and a low pressure drop. Shortening the monolith length is desirable due to the existence of the developing laminar flow at a longer distance from the channel inlet. Therefore, the heat transfer is more intense [9], but on the other hand, the flow resistance is enhanced as well. The validity of this approach has been confirmed by many subsequent works [10–14]. Short-channel structures combine much more intense heat transfer properties than monoliths with a slight increase in flow resistance. Although short-channel structures do not ensure both the heat/mass transport intensity of packed beds and a flow resistance similar to the one generated by monoliths, these properties can be largely adjusted to the required parameters of a specific process.

Not only is the length of the structure important, but also the shape of the channel cross-section [9]. Comparison of the values of transport and flow parameters (such as Nusselt number Nu and $f \cdot Re$ -Fanning friction factor multiplied by Reynolds number) for fully developed flow indicates the more favorable properties of hexagonal shapes than of square and triangular ones [8,15–20]. There are few publications concerning hexagonal channels, and most of them are based on CFD (computational fluid dynamics) [16,17]. Typically, the flow through the catalytic support itself is modeled. Recently, works have been appearing that investigate the behavior of the fluid when it flows into the channels of the monolith, as well as when it flows out of the channels. Cornejo et al. [21] studied the pressure drop through a honeycomb substrate for several channel shapes, including a hexagonal one. As the authors suggested, the reduction in the flow area entering the substrate produces a non-flat velocity profile at the channel's inlet.

Therefore, this paper presents the experimental and numerical results of the flow resistance of short-channel structures of hexagonal cross-section shape. A comparison of the obtained results with the literature dealing with such reactor internals is also carried out.

2. Theoretical Background

The flow resistance can be expressed as the Fanning friction factor f calculated with the use of the Darcy–Weisbach equation:

$$\frac{\Delta P}{L} = 2 \cdot f \cdot \frac{\rho \cdot u_0^2}{\varepsilon^2 \cdot D_h} \quad (1)$$

where D_h is the hydraulic diameter (m), defined as:

$$D_h = \frac{4 \cdot \varepsilon}{S_v} \quad (2)$$

The Fanning friction factor f can be determined in terms of the hydrodynamically dimensionless channel length L^+ :

$$L^+ = \frac{L}{D_h \cdot Re} \tag{3}$$

Table 1 contains the literature solutions describing the flow resistance in a hexagonal duct. Although Hawthorn [22] developed a semi-empirical equation for a circular duct, as the author suggested, the proposed equation can also be valid for channels of different cross-sections by substituting the appropriate $(f \cdot Re)_{fd}$ value for the duct under consideration. The values of $(f \cdot Re)_{fd}$ presented in the literature on hexagonal channels differ slightly (15.054 [8], 15.065 [16], 15.077 [17], 14.974 [18]); therefore, $(f \cdot Re)_{fd} = 15.054$ was introduced to Hawthorn’s [22] equation.

Table 1. Literature models describing the fluid flow through a hexagonal duct.

Ref.	Correlation	Notations
Hawthorn [22]	$(f \cdot Re) = (f \cdot Re)_{fd} \cdot \left(1 + \frac{0.045}{L^+}\right)^{0.5}$	$(f \cdot Re)_{fd} = 15.054$
Asako et al. [16]	$\frac{\Delta P}{\rho \cdot u^2} = (f \cdot Re)_{fd} \cdot \frac{4 \cdot L^+}{D_h \cdot Re} + K$	$(f \cdot Re)_{fd} = 15.065$ $K = 1.324$
Turgut [17] ¹	$(f \cdot Re) = (f \cdot Re)_{fd} + 0.03 \cdot (L^+)^{-1.01}$	$(f \cdot Re)_{fd} = 15.077$
Yilmaz [23]	$\frac{\Delta P}{\rho \cdot u^2} = 64 \cdot \psi \cdot L^+ + \frac{13.766 \cdot L^{+0.5}}{\left[1 + 13.95 \cdot \psi \cdot L^{+0.5} + \left(\frac{13.766}{K} \cdot 13.766\right)^3 \cdot L^{+1.5}\right]^{\frac{1}{3}}}$	$\Psi = 0.94$ $K = 1.426$
Muzychka and Yovanovich [24]	$(f_{app} \cdot Re \sqrt{A}) = \left[\left(\frac{12}{\sqrt{\varepsilon(1-\varepsilon)} \left[1 - \frac{192\varepsilon}{\pi^5} \cdot \tanh\left(\frac{\pi}{2\varepsilon}\right) \right] \right)^2 + \left(\frac{3.44}{\sqrt{L^+}} \right)^2 \right]^{1/2}$	$\mathcal{C} = b/a = 0.885$

¹ Correlation equation based on Figure 4b in [17].

3. Results and Discussion

Figure 1 shows the comparison of experimental results with literature models for 6 mm long short-channel structures of hexagonal channel cross-section shape.

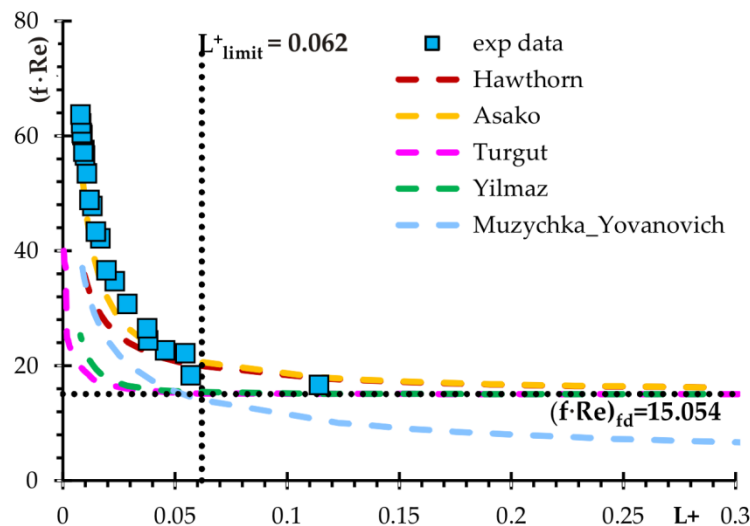


Figure 1. Comparison of experimental results with literature solutions for tested structure.

When comparing the experimental flow resistance values obtained for the structure tested with those in literature models, it is noticeable that they are in quite good agreement with Asako et al. [16] (relative error $e_y = 11.3\%$). Additionally, Turgut [17] found that $L^+_{limit} = 0.062$ is the limit value required to achieve a fully developed flow in a hexagonal

duct (depicted in Figure 1). As can be seen, after exceeding this value the flow resistance changes only slightly. Therefore, it can be assumed that the developing laminar flow exists in 6 mm long hexagonal channels in the tested range of L^+ .

It should be noted, however, that theoretical models (Table 1) consider simplified geometry: only the channel, without the regions before and behind it, is considered, hence only the viscous friction in the duct is taken into account. In practice, the drag resistance caused by the frontal surface of the wall thickness also exists, resulting in differences between the real flow and its theoretical predictions [9] (see Section 4, Materials and Methods). Therefore, the following equation was developed for hexagonal channels, assuming the viscous friction and the drag resistance:

$$(f \cdot Re) = 15.054 + 0.175 \cdot (L^+)^{(-1.19)} \quad (4)$$

which describes experimental results with relative error $e_y \approx 7\%$, as presented in Figure 2. The proposed correlation (4) has the same scheme as solutions for ducts with other cross-section shapes [10].

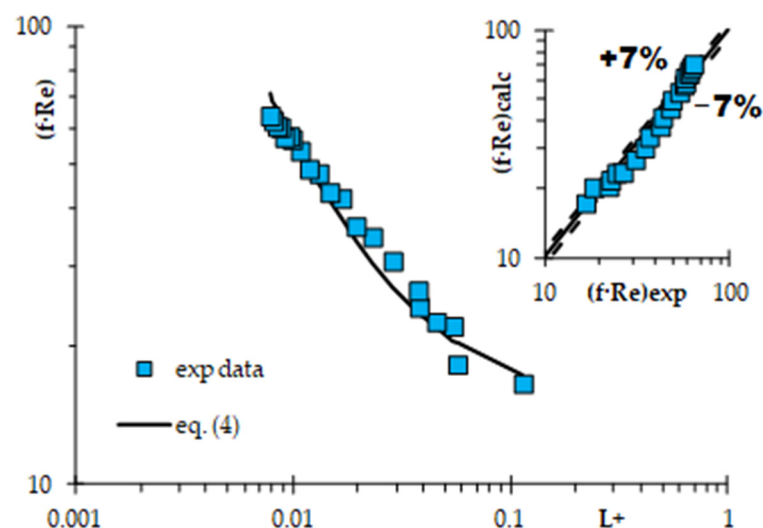


Figure 2. Flow resistance for hexagonal channel tested. Inset: parity plot for Equation (4).

Figure 3 shows the comparison of experimental and numerical results for two variants of channel geometry: ideal and real. Comparison of numerical approaches indicates the discrepancies between them, especially for higher values of Re . However, the real model (with non-zero wall thickness) displays good agreement with experimental data; the relative error of which is $e_y < 7\%$.

Additional results of numerical modeling are presented in Figures 4–6 as static pressure distribution along the computational domains of simplified and real models.

As can be seen in Figure 4, static pressure in front of the channel entrance is more than twice as large for real model than for simplified one. It can be seen that near the wall there is a little rise in pressure directly before entering the channel. Next, pressure values decrease at the channel entrance, especially in real model. This pressure drop is more significant near the wall, resulting in negative values of pressure (see Figure 4a). At the channel end, the pressure values are also negative, more so in the case of real model. When comparing the distribution of static pressure presented in Figures 5 and 6, it is noticeable that higher values of static pressure are obtained in real model before the channel inlet in the wall region than in simplified ones. At the channel entrance in real model, the highest pressure is located in the core of the channel, while the region close to the wall indicates some underpressure due to flow disturbances caused by vortices. In simplified model, this phenomenon is not observed because the gas enters the channel without changing the

flow passage (due to a lack of frontal surface area of wall), thus the highest pressure occurs near the channel wall. Moreover, a longer distance from the channel inlet is required in simplified models to stabilize the flow and hence the pressure (see Figure 5).

The computational simulations of flow resistance were also carried out for 1, 2 and 4 mm long hexagonal structures (Figure 7). Numerical modeling for these channels was performed only for the real models, due to the better agreement between the experimental data and the simulated real model for 6 mm long ducts. Figure 8 shows the comparison of the Fanning friction factor f obtained for different channel lengths with a long monolith ($L = 0.2$ m). Flow resistance in the monolith was described using the semi-empirical equation developed by Hawthorn [22].

As was expected, the shorter the channel length, the higher the flow resistance. The differences in pressure drop between structures decrease with the increasing channel length; the smallest difference is between the structures of $L = 4$ mm and $L = 6$ mm (Figure 7). As can be seen in Figure 7, hexagonal structures of 6 mm length lie the closest to the long monolith and are closer for low fluid velocities. The discrepancies between the long monolith and structures of different lengths rise up with u_0 . However, for all modeled lengths of the structure, the dependence of $f \cdot Re$ vs. L^+ follows one line, which is shown in Figure 8.

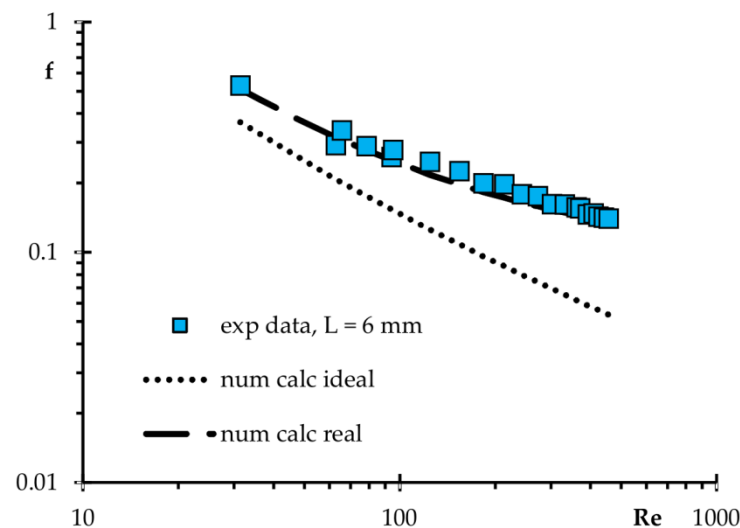


Figure 3. Comparison of numerical and experimental results for tested structure.

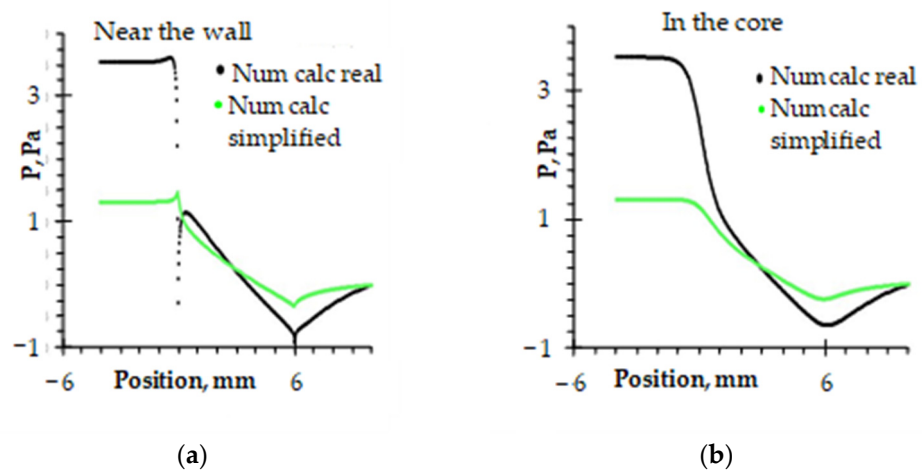


Figure 4. Comparison of static pressure along the computational domain between simplified and real models ($u_0 = 1 \text{ m} \cdot \text{s}^{-1}$): (a) near the wall; (b) in the core.

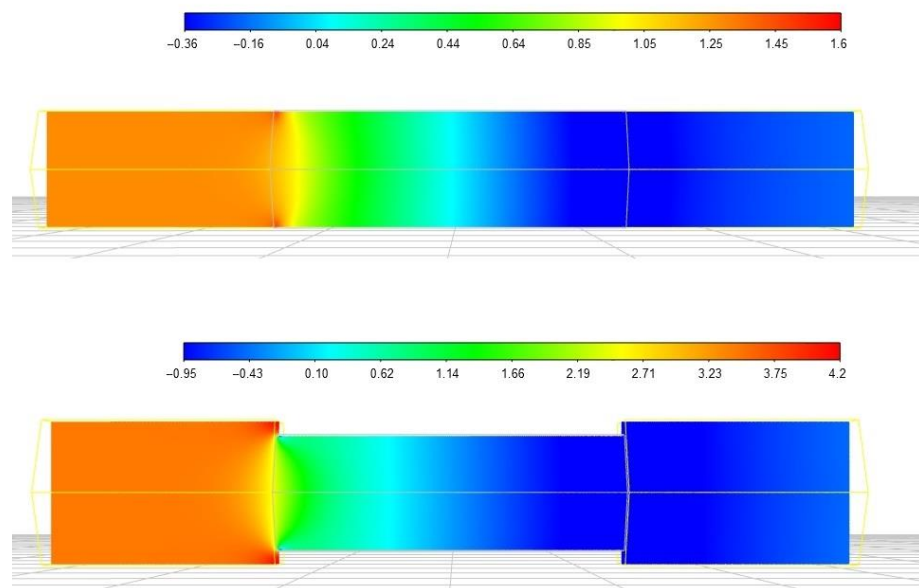


Figure 5. Distribution of static pressure along the computational domain for simplified (**top**) and real (**bottom**) models ($u_0 = 1 \text{ m}\cdot\text{s}^{-1}$).

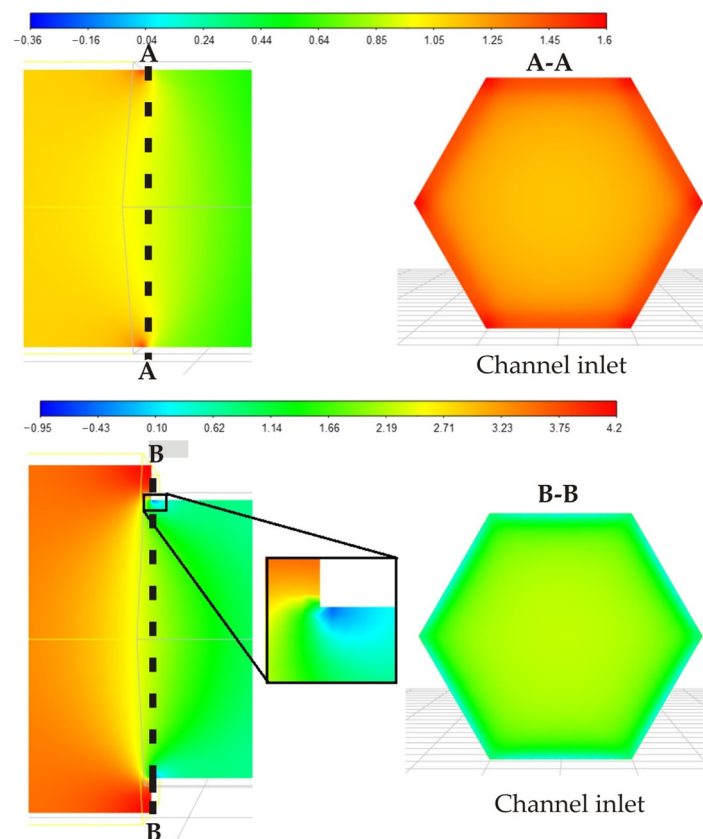


Figure 6. Distribution of static pressure at the channel entrance for simplified (**top**) and real (**bottom**) models ($u_0 = 1 \text{ m}\cdot\text{s}^{-1}$).

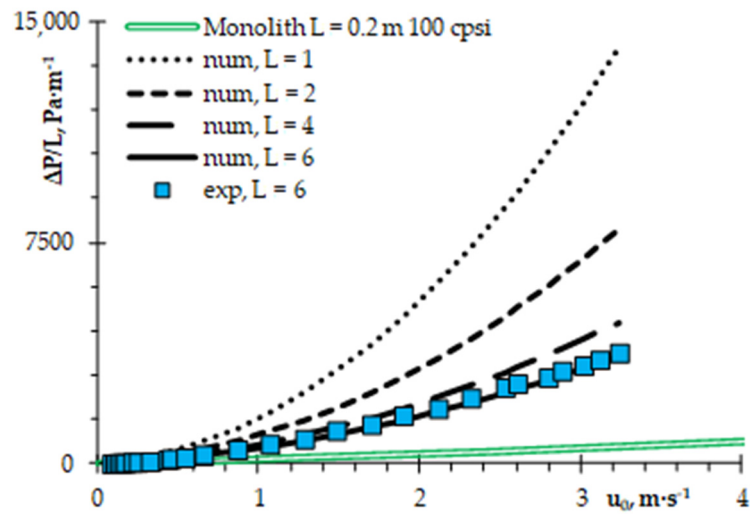


Figure 7. Comparison of numerical results for different channel lengths.

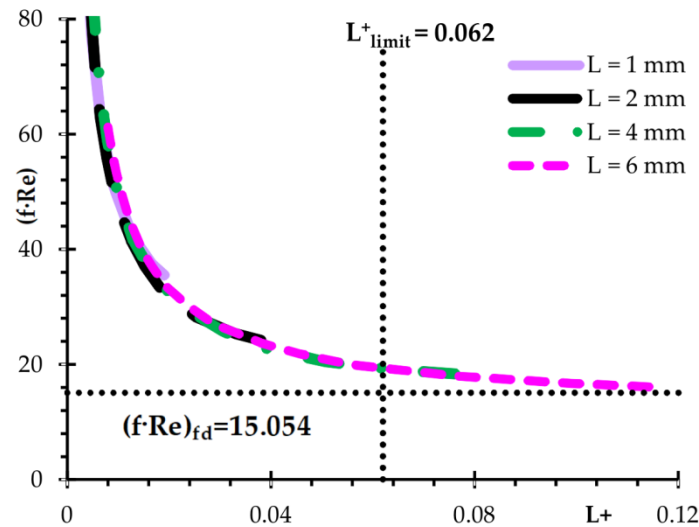


Figure 8. $f \cdot Re$ vs. L^+ for different channel lengths.

4. Materials and Methods

4.1. Experimental Set-Up

The pressure drop was determined for a 6 mm short-channel structure of hexagonal cross-section shape, with $S_v = 1743.66 \text{ m}^2 \cdot \text{m}^{-3}$ and porosity $\varepsilon = 0.73$. Images together with the dimensions are shown in Figure 9. It was manufactured from 316 stainless steel using the SLM (selective laser melting) method. The experimental setup is shown in Figure 10.

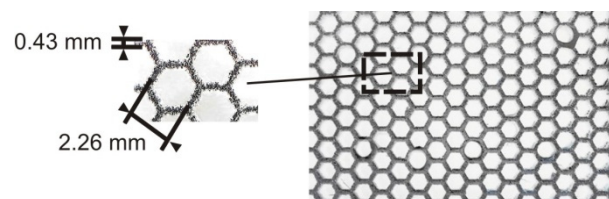


Figure 9. Sample's characteristic dimensions.

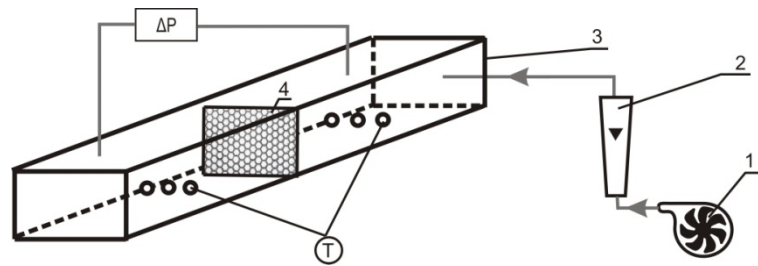


Figure 10. Experimental setup: 1-blower, 2-rotameter, 3-reactor, 4-sample, T-thermocouples.

Reactor with rectangular test section of 30×45 mm was used to carry out the pressure drop measurement. The sample was placed in the reactor perpendicular to the flow direction. All experiments were conducted in ambient air conditions; fluid velocity was changed in the range from 0.2 to $3.2 \text{ m}\cdot\text{s}^{-1}$ (which corresponds to Reynolds numbers Re from 30 to 450). Air temperature was measured by three thermocouples at the inlet and outlet sides. Recknagel micromanometer was used for pressure drop measurements.

4.2. Numerical Method

CFD analysis was carried out using ANSYS Fluent 20.2 software. A single channel of 6 mm length (Figure 11) was modeled to reduce the CPU usage and simulation time. Laminar flow was chosen according to Reynolds numbers evaluation (below 500). The pressure–velocity coupling formulation of the SIMPLE algorithm was adopted using a second-order upwind scheme. Velocity-inlet and pressure-outlet boundary conditions were employed at the inlet and outlet, respectively. To attain convergence, the continuity and momentum equations were iterated until the residuals fell below 1×10^{-3} .

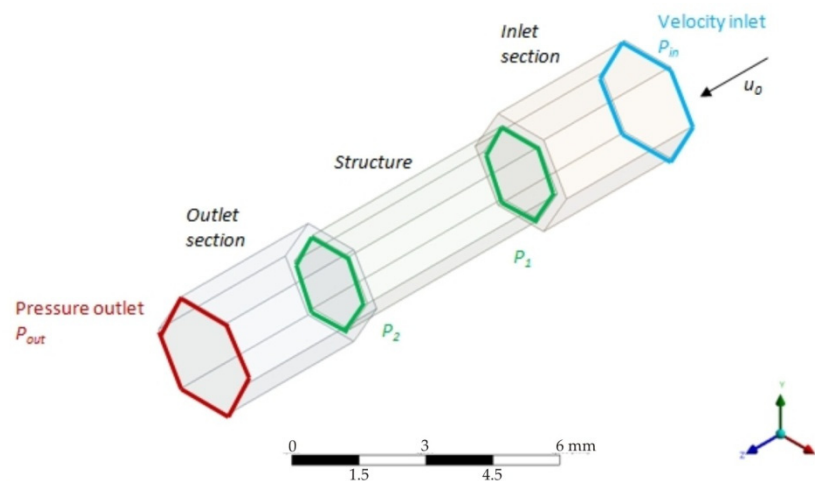


Figure 11. Computational domain of real model with boundary conditions for pressure drop calculation.

The continuity and momentum equations are as follows, respectively:

$$\nabla \cdot \vec{u}_0 = 0 \quad (5)$$

$$\rho \vec{u}_0 \nabla \cdot \vec{u}_0 = -\nabla p + \mu \nabla^2 \vec{u}_0 \quad (6)$$

Pressure drop ΔP was calculated as a mass-weighted average over the cross-sections referred to as P_{in} and P_{out} (Figure 11). From the boundary condition imposed at the outlet, the static pressure (P_{out}) is always zero. Therefore, the pressure drop through the channel corresponds to the pressure value measured at the inlet section. As was stated earlier (see

Section 3, Results), the theoretical models (Table 2) consider only flow through the channel, omitting the drag force resulting from frontal surface area of channel wall; thus, pressure drop should be calculated as a mass-weighted average over the cross-sections referred to as P_1 and P_2 (see Figure 3). Therefore, during the numerical modeling, the pressure drop was analyzed in two ways: (1) containing only viscous friction, referred to as the “simplified” model, and (2) including also drag force, referred to as the “real” model; more details about both models can be found in [9].

Table 2. Mesh convergence.

Model		No Elements	P_{in}, Pa	e_y
Simplified	1	538,720	7.2572	22.3604788
	2	621,600	5.9367	0.09610521
	3	704,480	5.931	-
Real	1	1,168,090	21.926	0.19192104
	2	1,432,270	21.887	0.01370865
	3	1,701,770	21.884	-

The computational domain consisted of hexahedral elements; the procedure for grid preparation and its distribution is described in detail in [9]. The mesh independence study was performed by changing the cell size inside the computational domain until the variation in pressure drop was less than 0.1%. The results obtained with different mesh sizes are given in Table 2 and Figure 12 for $u_0 = 3$ (m·s⁻¹).

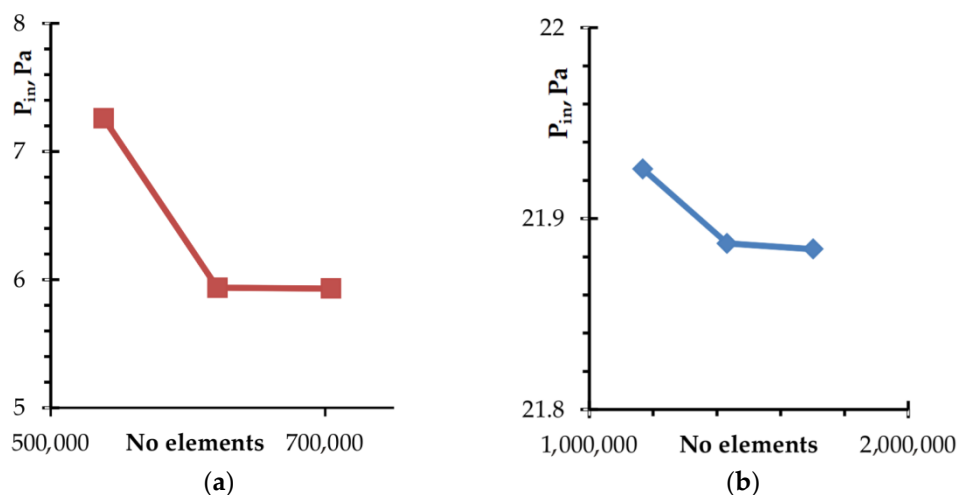


Figure 12. Mesh convergence for simplified (a) and real (b) models.

5. Conclusions

The comparison of results obtained for hexagonal structures tested with theoretical solutions indicated some differences resulting from the approach of neglecting the channel wall thickness. Numerical analyses allowed the identification of the differences in pressure distribution in the two models considered (simplified and real). It is highly recommended to take under consideration the frontal surface area (real model) in overall flow resistance. The channel wall thickness contributes the drag force, and thus the gas flow is disturbed [9]. For this reason, the static pressure at the channel entrance reaches higher values than in the case of the simplified model, and the occurrence of negative pressure near the wall causes the high pressure drop.

While some theoretical models reflect the experimental data, it seems more accurate to include the channel wall thickness in modeling and describing the flow resistance. Only the real model provides a detailed analysis of fluid flow phenomena.

Author Contributions: Conceptualization, M.I.; experimental analysis, K.S.; CFD analysis, M.I.; writing—original draft preparation, M.I. and K.S.; writing—review and editing, P.J.J.; funding acquisition, P.J.J. All authors have read and agreed to the published version of the manuscript.

Funding: This research was funded by National Centre for Research and Development (Project LIDER/204/L-6/14/ NCBR/2015).

Conflicts of Interest: The authors declare no conflict of interest.

List of Symbols

K	according to [16] or [23]
L	sample thickness. m
Re	Reynolds number = $u_0 \cdot D_h \cdot \rho \cdot \mu^{-1} \epsilon^{-1}$
$Re_{\sqrt{A}}$	according to [24]
S_v	specific surface area. $m^2 \cdot m^{-3}$
u_0	superficial fluid velocity. $m \cdot s^{-1}$
ΔP	pressure drop. Pa
ϵ	porosity
μ	dynamic viscosity, Pa·s
ρ	density. $kg \cdot m^{-3}$
Ψ	according to [23]
<i>Subscripts</i>	
fd	fully developed
app	apparent

References

- Loomis, D.; Grosse, Y.; Lauby-Secretan, B.; El Ghissassi, F.; Bouvard, V.; Benbrahim-Tallaa, L.; Guha, N.; Baan, R.; Mattock, H.; Straif, K. The carcinogenicity of outdoor air pollution. *Lancet Oncol.* **2013**, *14*, 1262–1263. [CrossRef]
- Hamra, G.B.; Guha, N.; Cohen, A.; Laden, F.; Raaschou-Nielsen, O.; Samet, J.M.; Vineis, P.; Forastiere, F.; Saldiva, P.; Yorifuji, T.; et al. Outdoor Particulate Matter Exposure and Lung Cancer: A Systematic Review and Meta-Analysis. *Environ. Health Perspect.* **2014**, *122*, 906–911. [CrossRef] [PubMed]
- Dumesic, J.A.; Huber, G.W.; Boudart, M. Principles of Heterogeneous Catalysis. In *Handbook of Heterogeneous Catalysis*; Wiley: Hoboken, NJ, USA, 2008.
- Pardiwala, J.; Patel, F.; Patel, S. Review paper on Catalytic Converter for Automotive Exhaust Emission. In Proceedings of the International Conference on Current Trends in Technology, Ahmedabad, India, 8–10 December 2011.
- Williams, J.L. Monolith structures, materials, properties and uses. *Catal. Today* **2001**, *69*, 3–9. [CrossRef]
- Kołodziej, A.; Łojewska, J. Short-channel structured reactor for catalytic combustion: Design and evaluation. *Chem. Eng. Process. Process. Intensif.* **2007**, *46*, 637–648. [CrossRef]
- Kołodziej, A.; Łojewska, J.; Ochońska, J.; Łojewski, T. Short-channel structured reactor: Experiments versus previous theoretical design. *Chem. Eng. Process. Process. Intensif.* **2011**, *50*, 869–876. [CrossRef]
- Shah, R.K.; London, A.L. *Laminar Flow Forced Convection in Ducts*; Academic Press: New York, NY, USA, 1978.
- Iwaniszyn, M.; Jodłowski, P.J.; Sinderka, K.; Gancarczyk, A.; Korpyś, M.; Jędrzejczyk, R.J.; Kołodziej, A. Entrance effects on forced convective heat transfer in laminar flow through short hexagonal channels: Experimental and CFD study. *Chem. Eng. J.* **2021**, *405*, 126635. [CrossRef]
- Iwaniszyn, M.; Piątek, M.; Gancarczyk, A.; Jodłowski, P.; Łojewska, J.; Kołodziej, A. Flow resistance and heat transfer in short channels of metallic monoliths: Experiments versus CFD. *Int. J. Heat Mass Transf.* **2017**, *109*, 778–785. [CrossRef]
- Iwaniszyn, M.; Kryca, J.; Jodłowski, P.J.; Piątek, M.; Gancarczyk, A.; Łojewska, J.; Kołodziej, A. Novel intense metallic monolith for automotive applications: Experimental versus numerical studies. *C. R. Chim.* **2015**, *18*, 1030–1035. [CrossRef]
- Iwaniszyn, M.; Ochońska, J.; Gancarczyk, A.; Jodłowski, P.; Knapik, A.; Łojewska, J.; Janowska-Renkas, E.; Kołodziej, A. Short-Channel Structured Reactor as a Catalytic Afterburner. *Top. Catal.* **2013**, *56*, 273–278. [CrossRef]
- Iwaniszyn, M.; Ochońska, J.; Jodłowski, P.; Łojewska, J.; Kołodziej, A. Very short monoliths of triangular cross-sectional channel shape for fast catalytic reactions. *Przem. Chem.* **2012**, *91*, 1435–1438.
- Kołodziej, A.; Łojewska, J.; Iwaniszyn, M.; Jodłowski, P.; Ochońska, J.; Rogulska, A.; Gancarczyk, A.; Matuszek-Chmuruwska, A. Mass transfer and flow resistance for sinusoidal short-channel catalytic internals. *Przem. Chem.* **2012**, *91*, 2074–2078.
- Shah, R. Laminar flow friction and forced convection heat transfer in ducts of arbitrary geometry. *Int. J. Heat Mass Transf.* **1975**, *18*, 849–862. [CrossRef]
- Asako, Y.; Nakamura, H.; Faghri, M. Developing laminar-flow and heat-transfer in the entrance region of regular polygonal ducts. *Int. J. Heat Mass Transf.* **1988**, *31*, 2590–2593.

17. Turgut, O. Numerical investigation of laminar flow and heat transfer in hexagonal ducts under isothermal and constant heat flux boundary conditions. *Iran. J. Sci. Technol. Trans. Mechan. Eng.* **2014**, *38*, 45–56.
18. Sadasivam, R.; Manglik, R.M.; Jog, M.A. Fully developed forced convection through trapezoidal and hexagonal ducts. *Int. J. Heat Mass Transf.* **1999**, *42*, 4321–4331. [[CrossRef](#)]
19. Gu, S.; Lu, T.; Evans, A. On the design of two-dimensional cellular metals for combined heat dissipation and structural load capacity. *Int. J. Heat Mass Transf.* **2001**, *44*, 2163–2175. [[CrossRef](#)]
20. Othman, M.Y.H.; Hussain, F.; Sopian, K.; Yatim, B.; Ruslan, H. Performance Study of Air-based Photovoltaic-thermal (PV/T) Collector with Different Designs of Heat Exchanger. *Sains Malays.* **2013**, *42*, 1319–1325.
21. Cornejo, I.; Nikrityuk, P.; Hayes, R.E. The influence of channel geometry on the pressure drop in automotive catalytic converters: Model development and validation. *Chem. Eng. Sci.* **2020**, *212*, 115317. [[CrossRef](#)]
22. Hawthorn, R.D. Afterburner Catalysis-Effects of Heat and Mass Transfer between Gas and Catalyst Surface. In *Proceedings of the AIChE Symposium Series*; American Institute of Chemical Engineers: New York, NY, USA, 1974; pp. 428–438.
23. Yilmaz, T. General Equations for Pressure Drop for Laminar Flow in Ducts of Arbitrary Cross Sections. *J. Energy Resour. Technol.* **1990**, *112*, 220–223. [[CrossRef](#)]
24. Muzychka, Y.S.; Yovanovich, M.M. Laminar Forced Convection Heat Transfer in the Combined Entry Region of Non-Circular Ducts. *J. Heat Transf.* **2004**, *126*, 54–61. [[CrossRef](#)]